Design and Performance of the Axial Ring-Cusp Hybrid (ARCH) Discharge for Miniature Ion Thrusters

IEPC-2017-295

Presented at the 35th International Electric Propulsion Conference
Georgia Institute of Technology – Atlanta, Georgia – USA
October 8–12, 2017

Ben Dankongkakul*
Air Force Research Laboratory, Edwards AFB, CA, 93515, USA

Richard E. Wirz†
University of California, Los Angeles, 90025, USA

Abstract: The miniaturization of traditional ring-cusp discharges is restricted by the increased surface area-to-volume ratio that reduces the primary electron confinement time necessary for efficient plasma generation. The ARCH discharge design decouples primary and plasma electron losses, in a manner similar to a Kaufmann and Magneto-Electric discharges, while maintaining the advantages of using ring-cusp designs. Discharge mapping and performance testing of the Axial Ring-Cusp Hybrid (ARCH) discharge demonstrate favorable plasma conditions within the discharge and near the extraction plane. These results suggest that the current 3 cm implementaion of the ARCH discharge can potentially achieve discharge losses and mass utilization efficiencies of 175 W/A and 0.87, respectively. As such, the new ARCH design approach may allow miniature ion thrusters to achieve the performance and efficiency levels similar those of highly efficient conventional ion thrusters.

I. Introduction

Miniature ion thrusters offer a highly efficient form of space propulsion that is an attractive option for attitude control in medium-size spacecraft or for orbit transfer in smaller spacecraft.[1] The plasma generation or discharge chamber in larger-scale ion thrusters (>10 cm) have been well understood and optimized through decades of research and development.[2] Most modern DC ion thrusters have adopted the ring-cusp design using permanent magnets to generate strong cusp confinement boundaries near the walls while the bulk plasma remains relatively unmagnetized for uniform plasma generation. At the miniature scale, many conventional design principles become difficult to implement. The multiple ring-cusps produce complex and strong magnetic field structures that dominate most of the chamber volume. In addition, the miniaturization of ion thruster discharge have been accompanied by low discharge efficiencies due largely to the inherent increase to the surface area-to-volume ratio of the plasma generation chamber and decrease confinement length of the primary electrons.[3–5]

To better understand the behavior of miniature discharge, we previously used the 3 cm Miniature Xenon Ion (MiXI) thruster as a platform to characterize several magnetic fields and miniature discharge configurations through discharge maps analyses and simulated performance measurements.[6] The full spatial measurements of the plasma parameters, including the electron energy distribution function (EEDF), provided insight into the discharge behavior of miniature-scale discharges. Combining these results with early observations allowed us to identify three key challenges for miniature ring-cusp ion thruster discharges:

1. The radially magnetized ring-magnets that are arranged around the cylindrical walls inherently generates very strong magnetic field gradients along the radial direction. This usually results in a strong

*Research Engineer, ERC Inc., bendankongkakul@ucla.edu.
†IAssociate Professor, Mechanical & Aerospace Engineering, wirz@ucla.edu.

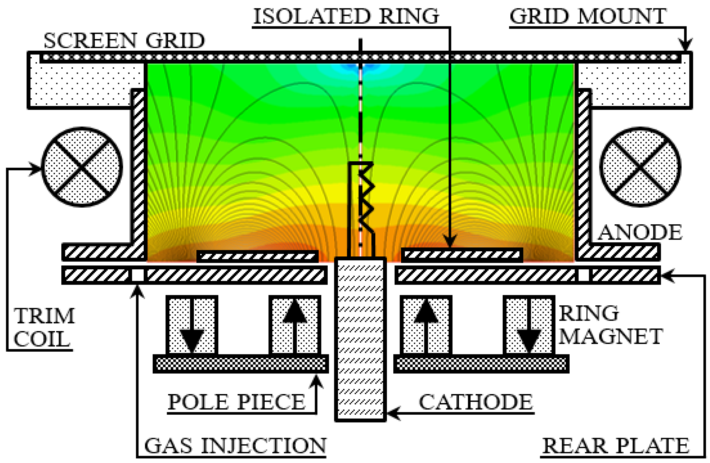

Figure 1. Diagram of the 3 cm diameter ARCH discharge with the key components labeled and overlaid with the magnetic field contour (in logarithmic scale).

plasma density gradient along the extraction plane, leading to poor beam flatness that is detrimental to the discharge performance and lifetime of the grid system.

2. Magnetic ring-cusps at anode potential directly exposed to the plasma will lead to high primary electron loss to the walls because of the small discharge volume.

3. Reducing the number or increasing the strength of the ring-cusps in order to improve the primary electron confinement leads to a reduced performance from over-confinement of the plasma electrons. High discharge voltages were required to extract a discharge current from the filament within a reasonable heater power.

The challenge for miniature discharge design is to address all three with a single design. One consideration is to consider a Kaufmann-style DC discharge which is known to provide high confinement efficiency for the primary electrons. This design is commonly used for terrestrial ion sources due to their reliability and heritage, but they require relatively high discharge voltages which results in lower lifetime and performance.

In this paper, we present a new approach to miniature discharge design called the Axial Ring-Cusp Hybrid (ARCH) discharge. Initial implementation exhibits plasma discharge efficiencies at the miniature scale that approach those of conventional large-scale ring-cusp ion thrusters. In the following sections, we first discuss the design and the basic operating principle of the ARCH discharge. Then we describe experimental efforts to measure the discharge performance via simulated ion thruster performance. These results show that the ARCH discharge can deliver over 2.5 times the ion current to the extraction plan compared to the original 3-ring cusp discharge for the same discharge power. The full plasma parameter map of the discharge chamber is then used to describe the unique plasma structure and behavior of the ARCH discharge.

II. ARCH Discharge

The ARCH discharge combines features of both Kaufmann and ring-cusp magnetic field designs with similarities to Magneto-Electrostatic discharges. Figure 1 shows that the magnetic field lines of this device resemble an arch structure and the “Axial Ring-Cusp” refers to placement and magnetization of the permanent magnets. There are three key aspects to the ARCH discharge design that address the miniaturization challenges previously discussed.

1. The permanent ring magnets are placed upstream of the discharge chamber with a predominately axial magnetization. This configuration generates a strong magnetic field gradient in the axial direction compared to the radial direction in conventional ring-cusp discharges. This approach generates a relatively low and uniform magnetic field strength across the majority of the extraction plane.

2. The concentric ring-cusps terminates at the upstream wall of the discharge chamber which is biased

below cathode potential. The non-collisional primary electrons generated at the discharge cathode are trapped in the arch-shaped magnetic fields and are unable to diffuse towards the anode.

3. The outer ring-cusp produces a moderate edge magnetic field that roughly parallels the cylindrical side walls and shields the anode of any direct leak path for the primary electrons. The collisional plasma electrons are able to diffuse across the edge fields to maintain the discharge current at reasonable discharge voltages.

A 5 mil tungsten filament was used for the discharge cathode and Xenon gas was introduced into the chamber through injection ports around the edge of the chamber. High-temperature trim coils with fiberglass insulation were wrapped directly around the discharge chamber to adjust the strength of the edge magnetic field. The magnetic field contours in fig. 1 are computationally generated and verified through Gaussmeter measurements shown in fig. 2. In the current design, there was an isolated inter-cusp ring in between the concentric ring-cusps that prevent a“short-circuiting” of the inter-cusp region.

III. Experimental Approach

The ARCH discharge testing was conducted using a 20” diameter by 36” height bell-jar vacuum chamber at the UCLA Plasma & Space Propulsion Lab. Xenon gas was injected into the chamber through an electrically isolated gas feed line. Probes were mounted onto a set of orthogonally mounted linear stages configured to raster along an azimuthal slice of the discharge chamber. All measurements were recorded using a DAQ module that featured a 300 V_{rms} channel-to-ground isolation. More details of the approach and methodology described in section III.A and III.B can be found in ref. [6].

A. Simulated Ion Thruster Performance

The ARCH discharge tests were performed using the MiXI thruster platform and grids.[7,8] The MiXI grids were designed for plasma densities of approximately $\sim 2 \times 10^{17}$ m^{-3} just upstream of the extraction plane. In order to focus on discharge design and reduce the influence of the grid design, the discharge was characterized without beam extraction using a simulated ion thruster or “discharge-only” operation. The predicted performance for the simulated discharge was determined based on a simple model described by Brophy.[9] This methodology has previously been implemented by several researchers on different ion thrusters and have been shown to reliably predict the discharge performance.[6,10,11]

The discharge performance data were measured by keeping the discharge voltage constant and slowly increasing the discharge current by adjusting the cathode filament heater power. The performance results were calculated with assumptions based on operational data of the original 3-ring MiXI thruster with beam extraction, shown in table 1.[6,12] These parameters assume a 1100 V beam voltage, grids with 75% ion transparency, no beam divergence, and negligible doubly-charged ion population.[13] The performance data also does not include possible additional power usage and/or gas flow for the discharge and neutralizer cathode. The beam profile and flatness parameter is extrapolated using plasma parameters from the internal discharge maps for the simulated ion thruster.

Parameter	Values
Beam voltage	1089 V
Beam current	28.3 mA
Discharge voltage	25 V
Discharge current	0.503 A
Flow rate	0.51 SCCM
Discharge loss	444 eV/ion
Propellant Efficiency	0.79
Total Efficiency	0.56

Table 1. Performance data for the original 3-ring MiXI thruster calculated from the total extracted ion beam and beam profile.[4]

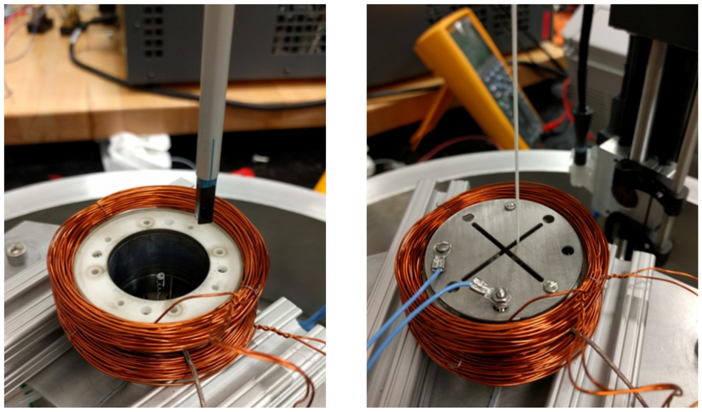

Figure 2. Left: The MiXI thruster without screen and accelerator grids and the Gaussmeter probe used to map the magnetic fields. Right: The device fitted with probing grids for 2D Langmuir probe mapping of the discharge plasma.

B. Discharge Mapping

To obtain maps of the discharge plasma, a set of stainless steel probing grids were installed in lieu of the original MiXI grids. These probing grids featured a 1.5 mm thin slit across the chamber diameter to allow the probe access to the discharge. To account for the increased neutral transparency, the gas flow rate was increased by a factor of 2.5 times to match the performance curves when operated using the MiXI grids. The Langmuir probe was able to access an entire azimuthal slice of the discharge chamber sans the region very near the cathode filament.

Plasma properties were measured using a cylindrical Langmuir probe, constructed with a 1.2 mm length by 0.2 mm diameter tungsten wire protruding from a 1.1 mm diameter alumina tube. Preliminary tests were used to confirm that the Langmuir probe did not significantly disturb the discharge plasma during operation. The Langmuir probe measurements were analyzed using standard probe theory for the plasma potential and electron temperature. The plasma potential was found at the maximum first derivative of the $I - V$ data. The second derivative data was used to calculate the electron temperature using a Maxwellian fit in the region near the floating point potential and avoiding the plasma potential as the low energy electrons are more affected by the magnetic fields. The plasma density was calculated from ion saturation data that are less affected by the magnetic fields. The Bernstein-Rabinowitz-Laframboise (BRL) theory was employed for the ion fit, which accounts for the effects of sheath expansion and ion orbital motion[14] for small diameter probes.

IV. Experimental Results

The ARCH discharge requires a start-up procedure to light the discharge plasma since, unlike a conventional ring-cusp, there was no direct anode path at the nominal operating condition. To address this, the anode was biased to >30 V at a typical operating flow rate. The rear plate was then biased positively towards ∼25 V or until a discharge current was measured at the anode, indicating the presence of plasma. Afterward, the rear plate was bias back down to sub-cathode potential and the anode was reduced to a nominal operating voltage (∼25 V). The filament heater was then adjusted to obtain the desired discharge current.

The device was tested at similar discharge conditions to the 3-ring discharge with the discharge voltage, screen grid, and accelerator grid biased to 25 V, -10 V, and 20 V, respectively.[6] A collector plate downstream of the thruster confirmed that there was negligible ion current leaving the discharge. Unless stated otherwise, a discharge voltage of 25 V was used; however, higher performance was often achieved at higher discharge voltages. Measurements were acquired once the discharge performance stabilized when thermal equilibrium was reached. The simulated operation was previously tested with the MiXI discharge and validated with beam extracted performance data.[6]

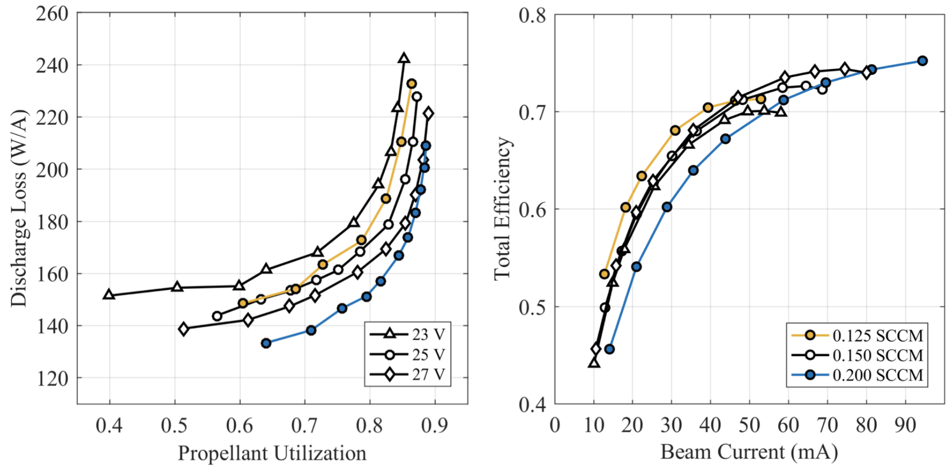

Figure 3. Performance assessment of the ARCH discharge at a range of discharge voltages and base neutral gas flow rates. The curves are generated by adjusting the heater power to increase the discharge current while keeping all other supplies constant.

A. Performance Data Analysis

The simulated performance data at a range of specified flow rates and discharge voltage are shown in fig. 3. The total efficiency in fig. 3b shows that the device is more efficient at lower flow rates when extracting lower beam currents and vis-versa. The performance also improves with increasing discharge voltages as it directly raises the primary electron energy and ionization rates. The opposite trend is observed in the 3-ring configuration due to low primary electron confinement. It should be noted that the total efficiency does not include many important factors that were previously discussed— the total efficiency only serves as a comparison metric with the 3-ring discharge.

Figure 4 is a comparison between 3-ring and the ARCH discharge. The red dot is the original 3-ring MiXI thruster's performance point shown in table 1. The ARCH cold is the performance curve measured at an operating temperature of $150 - 200°C$, before the anode reached thermal equilibrium at $\sim 480°C$. The filament cathode accounts for approximately two-thirds of the total power consumption that would be mostly absent when operated with a hollow cathode. In addition, the prototype was only designed to manage the temperature of the permanent magnets and not the anode. The higher temperatures lead to greater neutral

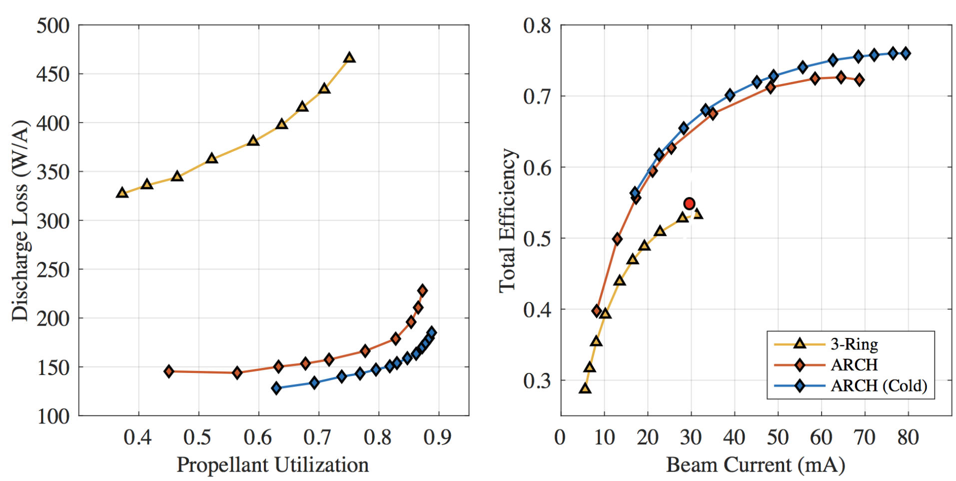

Figure 4. Performance comparison between the ARCH discharge and the original 3-ring configuration. Measurements are obtained for a 25 V discharge at 0.150 SCCM specified gas flow rate. The red circle represents operation with beam extraction from the conditions shown in table 1.

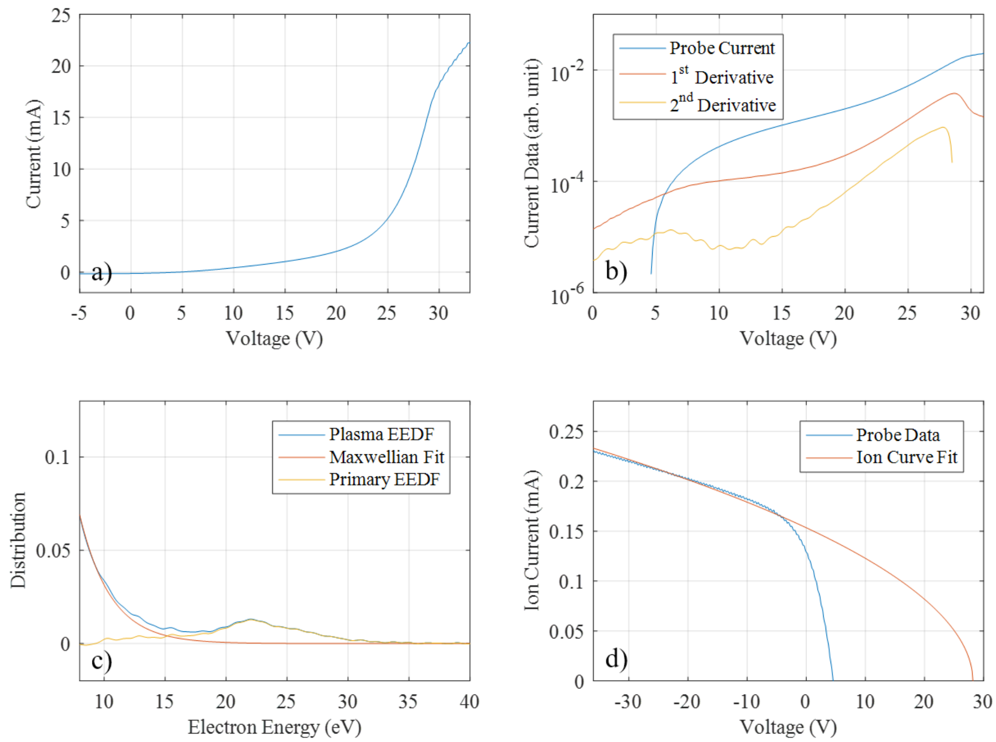

Figure 5. Example Langmuir probe data and analysis. (a) The binned then averaged I-V sweep. (b) The probe sweep and it's derivative plotted in a semi–log scale. (c) Extraction of the primary electron density through subtraction of a Maxwellian plasma electron population. (d) The ion saturation curve fitted using the BRL method.

velocities which decrease the neutral density by 20-25% for a given flow rate.

The beam current of the ARCH discharge is currently limited by the use of the MiXI grids, which were designed for lower plasma densities and beam current densities. However, at the 54 mA perveance limited beam current, it may be possible attain a discharge loss of under 160 eV/ion with a 0.85 propellant utilization efficiency. At 32 mA simulated beam current, which is ideal lifetime conditions for the MiXI grid system, it may be possible attain a discharge loss of under 180 eV/ion with a 0.82 propellant utilization efficiency. At the 3-ring MiXI thruster's nominal operating condition shown in table 1, the ARCH discharge is able to produce the same beam current at less than half the discharge power or over twice the beam current at a given discharge power.

B. Discharge Map Analysis

The four plots shown in fig. 5 are sample Langmuir probe data and analysis at an arbitrary location inside the discharge. The top right plot shows the standard $I-V$ trace in a semi-log plot along with the calculated first and second derivative. A higher energy electron population can be detected in the second derivative data by the kink in the curve at the higher energies. The bottom left figure shows the process of calculating the primary electron density. The primary electron population is defined as the difference between the full population and Maxwellian estimate for the plasma electrons. Although the Maxwellian fit may not match the data well at lower energies, the higher energy electrons are less affected by the magnetic fields. The bottom right plot shows the ion saturation fit using the BRL theory which iterates to a plasma density based on the sheath size.

The discharge maps shown in fig. 6 are interpolated contour plots of the plasma parameters for the ARCH discharge, operating at 0.35 A discharge current and 0.150 sccm specified flow. The average neutral density is $\sim 2 \times 10^{19}$ m^{-3} based on a control volume calculations between the specified flow rate and the total grid area. The plasma and primary electron density maps exhibit a double arch-like structure that strongly correlates with the magnetic field shape. The electron temperature ranges between 4 to 6 eV and exhibits a

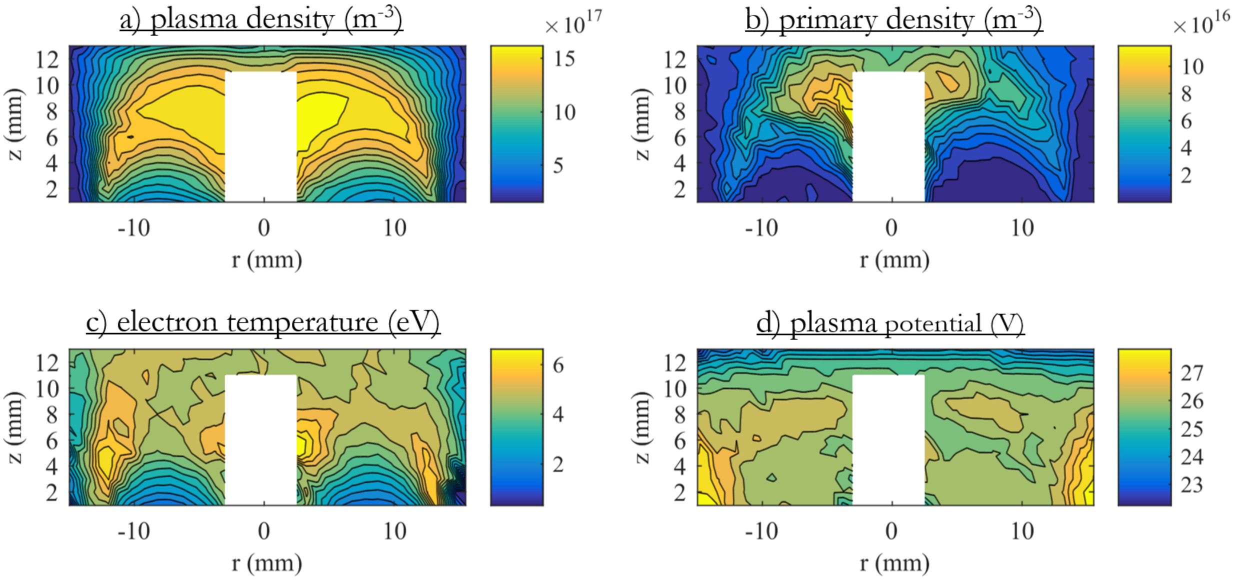

Figure 6. Discharge mapping results for the ARCH discharge showing the: a) plasma density (m^{-3}), b) primary electron density (m^{-3}), c) electron temperature (eV), and d) plasma potential (V). The cathode filament is located in the empty rectangular space at the center and is not probed. Note: the electron temperature values near the cusps are elevated as the Langmuir probe was oriented parallel to the strong cusp-fields

more gradual delineation compare to the density contours. The plasma potential within the entire discharge chamber is, by and large, uniform at ~ 26 V relative to the cathode potential.

Overall, the discharge maps show excellent overall confinement that verifies the simulated performance measurements. The plasma and primary electron are well distributed along and near the extraction plane for efficient ion generation. The primary electrons density contour shows that the population is well confined to the arch-shaped field lines; they easily diverge from the on-axis cathode source and are also unable to diffuse across the axial fields to the anode. At the outer ring-cusp, the primary electron lost width is on the order of their Larmor radius. In the bulk region, they are seen to have a toroidal or doughnut-like spatial distribution where the peak density is slightly off-axis — a formation that is favorable for efficient ion generation as the radial location corresponds to a larger grid area.

The electron temperature has the expected iso-thermal distribution along the magnetic field lines. The high electron temperature is an indication of good primary electron confinement as most of the discharge energy is deposited into the plasma through ionization or thermalization collision rather than lost to the walls. In addition, the primary electrons and temperature distributions are not localized to the center-line region that led to local neutral depletion and excessive double-ion generation such as in the NSTAR thruster.[7] It should be noted that the presented temperature values are most likely artificially elevated near the cusp region due to errors in the probe analysis. The z-axis orientation of the Langmuir probe in this region is parallel to the strong cusp magnetic field lines. This suppresses the electron collection and a more advance Langmuir probe theory would be required to better resolve the temperature in this region. In between the ring-cusps, the probe is oriented perpendicular to the field lines; the temperature values here are likely a more accurate representation of the temperature along the corresponding field lines.

The low plasma potential in comparison to the electron temperature indicates a minimal sheath potential where the ion and plasma electron loss are well balanced and most of the collected discharge current are the low-energy plasma electrons. Coupled with the low electron temperature along the anode, the net effect is a minimization of the plasma electron power loss to the walls from extracting the discharge current.

Figure 7 shows a comparison of the projected normalized beam profile, calculated from the plasma density and electron temperature values along the extraction plane. The 3-ring discharge has a notably flat beam profile even when compared to much large ion thrusters. The ARCH thruster features a slightly dipped beam profile and an estimated beam flatness of 0.66. Although slightly worse than the 3-ring discharge, it is still on par with most conventional-scale ion thrusters.

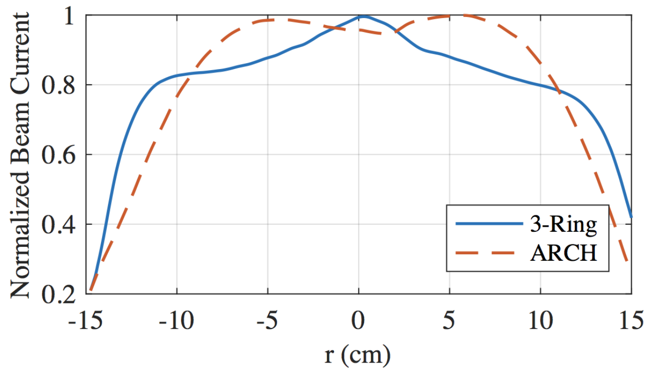

Figure 7. Normalized beam current profile, estimated from the plasma conditions measured near the exit plane of the discharge. Note: the beam current estimates are based on an ion transparency of 75% was assumed across the grid plane and grid perveance considerations are not included.

V. Conclusion

A highly efficient DC discharge design was developed that will allow miniature ion thrusters to obtain similar discharge performance to conventional-scale devices. Using MiXI thruster as a platform for simulated performance testing, the ARCH discharge was able to deliver over twice the ion current to the extraction plane compared to the 3-Ring discharge. The discharge mapping was also crucial to the initial design and subsequent improvements to the ARCH discharge. The mapping data provided insight into the discharge behavior through analysis of the plasma structure and allowed for assessment of the beam profile. In order to demonstrate full thruster operation, the next step will be to measure the ARCH discharge performance with beam extraction using the MiXI grids and hollow cathode.

Acknowledgments

This work was funded by the University of California, Los Angeles through the Dissertation Year Fellowship. The authors also acknowledge the valuable contributions by Taylor S. Matlock and the support of the Air Force Research Laboratory RQ-West.

References

[1]Wirz, R., Araki, S., and Dankongkakul, B., "Miniature Ion Thrusters: A Review of Modern Technologies and Mission Capabilities," *34th International Electric Propulsion Conference*, Hyogo-Kobe, Japan, July 2015, IEPC-2015-275.

[2]Wilbur, P. J., Rawlin, V. K., and Beattie, J. R., "Ion Thruster Development Trends and Status in the United States," *Journal of Propulsion and Power*, Vol. 14, No. 5, 1998, pp. 708–715.

[3]Tighe, W., Chien, K.-R., Ahn, J., Solis, E., Hurtado, J., and Spears, R., "Update on the XIPS 8-cm Thruster Prototype," *44th AIAA/ASME/SAE/ASEE Joint Propulsion Conference & Exhibit*, American Institute of Aeronautics and Astronautics, July 2008, AIAA-2008-4912.

[4]Wirz, R., Sullivan, R., Przybylowski, J., and Silva, M., "Hollow Cathode and Low-Thrust Extraction Grid Analysis for a Miniature Ion Thruster," *International Journal of Plasma Science and Engineering*, Vol. 2008, 2008, pp. 1–11.

[5]Dankongkakul, B., Araki, J., and Wirz, R., "Magnetic field structure influence on primary electron cusp losses for micro-scale discharges," *Physics of Plasmas*, Vol. 21, No. 043506, 2014.

[6]Dankongkakul, B. and Wirz, R. E., "Discharge Performance and Behavior of Miniature-Scale DC Ion Thruster Designs," *Journal of Applied Physics*, 2017, Accepted.

[7]Wirz, R. E., *Discharge plasma processes of ring-cusp ion thrusters*, Ph.D. thesis, California Institute of Technology, Pasadena, CA, 2005.

[8]Wirz, R. E., Polk, J., Marrese, C., Mueller, J., Escobedo, J., and Sheehan, P., "Experimental and Computational Investigation of the Performance of a Micro-Ion Thruster," *38th AIAA/ASME/SAE/ASEE Joint Propulsion Conference & Exhibit*, Indianapolis, Indiana, 2002, AIAA 2002–3835.

[9]Brophy, J. R., "Simulated ion thruster operation without beam extraction," *21st International Electric Propulsion Conference*, Orlando, Florida, 1990, IEPC-1990-2655.

[10]Goebel, D., Polk, J., and Sengupta, A., "Discharge Chamber Performance of the NEXIS Ion Thruster," *40th AIAA/ASME/SAE/ASEE Joint Propulsion Conference & Exhibit*, American Institute of Aeronautics and Astronautics, Fort Lauderdale, Florida, July 2004, AIAA-2004-3813.

[11]Foster, J. E., Hubble, A., Nowak-Gucker, S., Davis, C., Peterson, P., Viges, E., and Chen, D., "Simulated Beam Extraction Performance Characterization of a 50-cm Ion Thruster Discharge," *48th AIAA/ASME/SAE/ASEE Joint Propulsion Conference & Exhibit*, American Institute of Aeronautics and Astronautics, Atlanta, Georgia, July 2010, AIAA-2012-3795.

[12]Wirz, R. and Goebel, D., "Effects of magnetic field topography on ion thruster discharge performance," *Plasma Sources Science and Technology.*, Vol. 17, No. 3, Aug. 2008, pp. 035010.

[13]Wirz, R., "Computational Modeling of a Miniature Ion Thruster Discharge," *41st AIAA/ASME/SAE/ASEE Joint Propulsion Conference & Exhibit*, American Institute of Aeronautics and Astronautics, Tucson, Arizona, July 2005.

[14]Laframboise, J., *Theory of spherical and cylindrical Langmuir probes in a collisionless, maxwellian plasma at rest*, Ph.D. thesis, University of Toronto Institute for Aerospace Studies, 1966.